Journal of Physics D:
Applied Physics

PAPER • **OPEN ACCESS**

Influence of pulsed gas injections on the stability of Townsend dielectric barrier discharges in nitrogen at atmospheric pressure

To cite this article: L Cacot *et al* 2022 *J. Phys. D: Appl. Phys.* **55** 445204

OPEN ACCESS
IOP Publishing
Journal of Physics D: Applied Physics
J. Phys. D: Appl. Phys. **55** (2022) 445204 (15pp)
https://doi.org/10.1088/1361-6463/ac8e78

Influence of pulsed gas injections on the stability of Townsend dielectric barrier discharges in nitrogen at atmospheric pressure

L Cacot[1,3], G Carnide[1,2], M L Kahn[2], H Caquineau[1], R Clergereaux[1], N Naudé[1,*] and L Stafford[3,*]

[1] LAPLACE, Université de Toulouse, CNRS, INPT, UPS, Toulouse, France
[2] LCC, CNRS (UPR 8241), Université de Toulouse, 205 route de Narbonne, Toulouse 31077 Cedex 4, France
[3] Département de Physique, Université de Montréal, 1375 ave Thérèse-Lavoie-Roux, Montréal, QC H2V 0B3, Canada

E-mail: nicolas.naude@laplace.univ-tlse.fr and luc.stafford@umontreal.ca

Received 7 May 2021, revised 15 August 2022
Accepted for publication 1 September 2022
Published 12 September 2022

Abstract

This work investigates the effects of pulsed nitrogen gas injections on the stability of Townsend dielectric barrier discharges operated in continuous nitrogen gas flows at atmospheric pressure. For single-pulse injections with pulse durations lower than the continuous gas residence time (∼50 ms), current–voltage characteristics reveal homogeneous discharges with a single current peak per half-cycle of the applied voltage. However, a sudden decrease of the discharge power over time combined with a temporary transition from homogeneous to filamentary discharge is observed for longer pulses at fixed pulsed gas flows and for higher pulsed gas flows at fixed pulse duration. In addition, for multiple pulsed gas injections with repetition frequencies between 0.1 and 10 Hz, discharge destabilisation increases with the number of pulses. Time-resolved optical emission spectroscopy reveals that, over the single pulse time scale, temporal variations of the emission intensities are longer than the expected residence times of the continuous and pulsed gas flows. Furthermore, a rise of oxygen impurities can be seen over both single and multiple-pulses time scales. Two-dimensional gas flow simulations reveal that pulsed injections introduce sharp and narrow temporal gas velocity profiles over the range of experimental conditions investigated, with no cumulative effects in the discharge cell from one pulse to the other. However, pulsed operation introduces significant changes in the neutral gas composition with time scales comparable to those revealed by electrical and optical diagnostics. In such conditions, the outgassing of impurities adsorbed on surfaces located upstream of the discharge cell plays a vital role in Townsend discharges' physics and characteristics.

* Authors to whom any correspondence should be addressed.

Supplementary material for this article is available online

Keywords: dielectric barrier discharge, Townsend discharges, current–voltage characteristics, optical emission spectroscopy, pulsed gas injection

(Some figures may appear in colour only in the online journal)

1. Introduction

Non-equilibrium plasmas are routinely used in materials processing, for example, for thin film deposition and etching. For such applications, carrier and reactive gases are typically continuously injected in the plasma reactor [1, 2]. For selected applications, however, pulsed gas injections are more appropriate to ensure the right set of populations of plasma-generated species [3–5]. For example, pulsed precursor injections are implemented when an additional control over deposition rate and nanostructure is required. For instance, AlO_x thin film in a pulsed injection of $Al(CH_3)_3$ in an oxygen plasma tune from low-density after precursor injection (i.e. when the precursor concentration is high) to dense structure shortly after the injection (i.e. when the precursor concentration is low) due to the impingement of plasma-generated ions and reactive oxygen species on the substrate surface [6]. In hybrid plasma deposition processes relying on plasma-enhanced chemical deposition (PECVD) and sputtering, pulsed precursor injections can prevent target poisoning and can be used for the deposition of multifunctional, nanocomposite coatings [7, 8]. The pulsed carrier gas injections can also be synchronized with a pulsed power supply for discharge ignition and maintenance to precisely control the precursor dissociation and plasma-surface interactions during PECVD [9]. Nowadays, pulsed injections of the carrier, precursor, and reactive gases are also used in atomic layer deposition and atomic layer etching processes [10–12].

Compared to continuous gas flows, pulsed gas flows inevitably lead to temporal variations of the fundamental plasma properties. For example, in Tore Supra reactor used for fusion applications, the response of the scrape-off layer to a supersonic pulsed gas injection has shown an increase in the plasma density and a decrease in plasma temperature before returning to equilibrium after about 10 ms; in addition, the extent of such variations is proportional to the total amount of gas injected into the plasma [13]. In a capacitively-coupled, radio-frequency argon plasma at low pressure, Sadek *et al* [14] have reported cyclic evolutions of the electron temperature (T_e) and electron density (n_e) following the pulsed injection of neutral gas density in an argon plasma. Cyclic evolutions of T_e and n_e have also been reported by Garofano *et al* [15] with pulsed injection of hexamethyldisiloxane (HMDSO) in an argon plasma. In such conditions, variations of T_e and n_e are observed over multiple time scales: one linked to the pulsed injection of HMDSO in the argon plasma and another due to the successive formation and disappearance of nanoparticles in the dusty plasma [16, 17].

The effect of airflow on the space-time distribution of filaments in dielectric barrier discharge (DBD) at atmospheric pressure has also been investigated [18]. It is found that modification of the gas flow rate changes the breakdown positions and morphology of discharge filaments, a feature linked to the combined effect of electric field and airflow on particle distribution [19, 20]. While the filamentary regime of DBDs is more common, there has been significant interest in the so-called 'homogeneous' regime of DBDs characterized by the absence of micro-discharges and a relatively spatially homogeneous light emission over the whole inter-electrode gap [21, 22]. Of note, such micro-discharges in the filamentary regime of DBDs imply high-energy input localized over small surface areas such that their presence can be highly problematic for materials processing applications [23, 24]. On the other hand, homogeneous discharges can typically be obtained through judicious control of the voltage and current waveforms and the choice of the appropriate carrier and reactive gases [25].

A handful of studies have reported the development and use of homogeneous DBDs for advanced surface engineering applications (see, for example [26–35]). However, most of them implement continuous gas flows (carrier and precursor gases). This work aims to examine the effects of pulsed gas injections on the stability of homogeneous DBDs operated with a continuous laminar gas flow. To study the disturbances related to a pulsed injection, experiments are carried out with the injection of carrier gas only, without precursors. The experiments are done in the specific case of a low-density Townsend discharge obtained in a plane-to-plane configuration with N_2 for both the continuous and pulsed gas injections. As reported by many authors, this Townsend discharge is typically characterized by ion density $\sim 10^{10}$ cm^{-3}, electron density $\sim 10^{7}$ cm^{-3}, electron temperature $\sim$5 eV, neutral gas temperature $\sim$300 K, and power density in the $\sim$0.1–1 W cm^{-2} [21, 22]. Such Townsend discharges are relevant for the deposition of functional, nanostructured coatings on a variety of surfaces, including heat-sensitive materials [26–34]. Depending on the pulsed gas injection conditions, spatially-resolved current–voltage characteristics and time-resolved optical emission spectroscopy (OES) measurements reveal peculiar discharge behaviors following single and multiple pulsed gas injections.

2. Experimental set-up and diagnostics

The experimental setup used in this work was described in detail elsewhere [29, 31]. The plane-to-plane DBD cell is housed in an enclosed metallic chamber (volume below

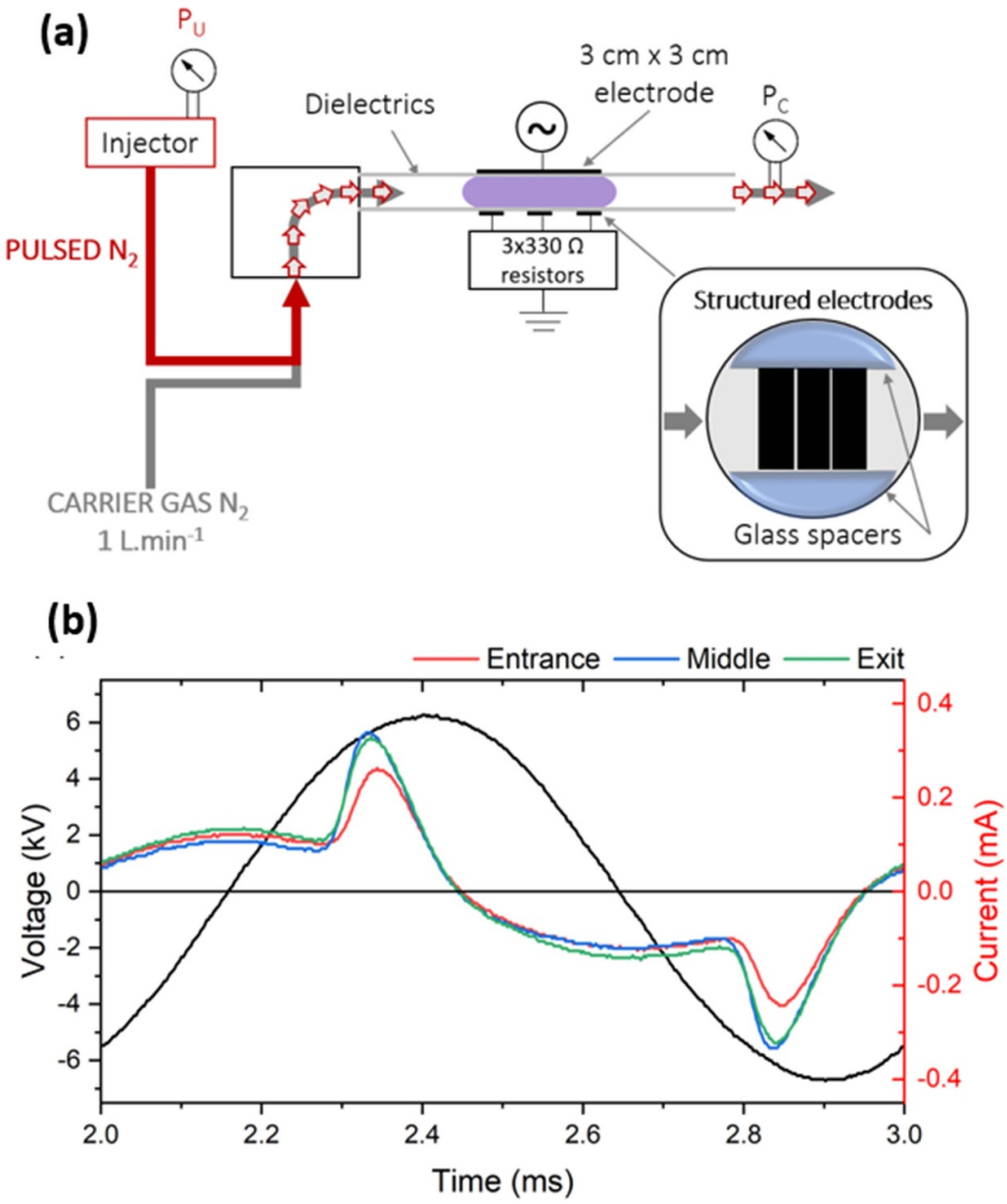

Figure 1. (a) Schematics of the experimental set-up with the multi-strip ground electrode for spatially-resolved electrical measurements; upstream of the DBD cell, the gas pipes for continuous and pulsed nitrogen gas flows arrive in a mixing chamber, (b) typical current–voltage characteristics of a Townsend discharge in N_2 at 1 kHz with a continuous gas flow.

100 cm^3) to carry out experiments in a controlled pressure and atmosphere. As shown in figure 1(a), the gas pipes (continuous and pulsed flows, see below) and DBD cell are connected in a gas mixing chamber. Downstream of the DBD, the system is linked to the vacuum system. Prior to each experiment, the chamber is pumped down to a pressure of 10^{-3} mbar to reduce any contamination. The gas gap is then filled up to atmospheric pressure by a continuous flow of N_2 (99.999% purity) at 1 l min^{-1}. The discharge cell consists of two parallel alumina plates separated by a 1 mm gap. One side of alumina plates is painted with a 3 cm $\times$ 3 cm conductive silver paste acting as a metallic electrode. To collect spatially resolved electrical measurements along the gas flow lines, the ground electrode is formed of three equal-size metalized strips; this feature is shown in figure 1(a) [36]. Here, the middle strip is separated by 400 μm from its neighbors.

A power supply providing a low-frequency sinusoidal voltage signal (1 kHz) is connected to a linear power amplifier whose output is linked to the primary winding of a step-up transformer. The discharge cell is connected to the secondary winding of the transformer. A 13 kV peak-to-peak voltage is applied to the electrodes and is measured by a high-voltage probe (Tektronix P6015A). The outputs of the three strips of the ground electrode are connected to three 330 Ω resistors to gather the corresponding currents. The applied voltage and measured currents of each zone are displayed on

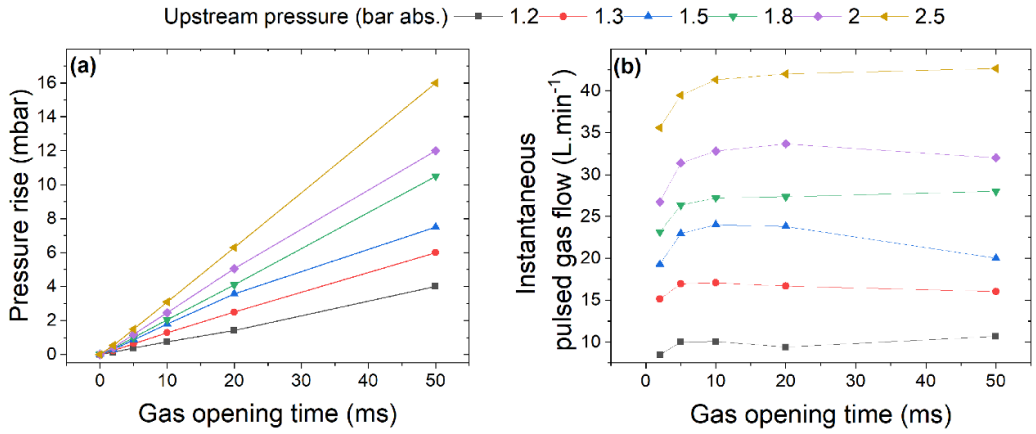

Figure 2. (a) Pressure variation (ΔP) inside the closed chamber as a function of the gas opening time (t_{gas}) for various upstream pressures (P_U). (b) Instantaneous pulsed gas flow (Q) as a function of gas opening time for various upstream pressures (P_U). In (a) and (b), lines are to guide the eye only.

an oscilloscope (Teledyne Lecroy WaveSurfer 3024, 200 MHz bandwidth).

Typical current–voltage characteristics of the Townsend discharge in N_2 at atmospheric pressure are presented in figure 1(b). Two specific features can be seen for all zones: (a) the sinusoidal portion linked to the displacement current and thus to time variations of the applied voltage, and (b) the broad peak associated to the discharge current in a homogeneous Townsend discharge [37–39]. Here, current densities in each zone are in the mA cm^{-2} range, which is consistent with other studies of low-frequency Townsend DBD [21, 22]. To obtain a homogeneous discharge rather than a filamentary discharge formed of narrow discharge channels randomly distributed in time and space [40], a Townsend (rather than streamer) breakdown is required [21]. This condition implies a preionization of the gas but also a discharge ionization slow enough to avoid a fast avalanche development. This can be achieved through the presence of long-lived species from one half-cycle of the applied voltage to the other; this effect is commonly referred to as the 'memory effect'. In the specific case of N_2 discharges, long-lived metastable N_2(A) states are not only involved in volume Penning ionization at low electric fields [41], but they can also induce secondary electron emission following their interaction with charged dielectric surfaces [42]. Over the range of experimental conditions examined, the very first discharges are typically filamentary and then become homogeneous due to the onset of memory effects linked to the formation of long-lived metastable N_2(A) states [41, 43].

In addition to the continuous gas flow, pulsed gas injection is realized using an Atokit injection system commercialized by Kemstream. The gas pulses are led to the discharge cell through a 60 cm long stainless-steel pipe with a 4 mm inner diameter. The pulsed gas is chosen identical to the continuous discharge gas (N_2, 99.999% purity). Several injection parameters can be controlled, including the gas opening time (pulse duration), the pulse injection frequency, and the gas pressure upstream of the pulsed injection device (upstream pressure, P_U, figure 1(a)). To maintain atmospheric-pressure conditions with both the continuous and pulsed gas flows, the pressure in the plasma chamber recorded at the output of the DBD cell is set to atmospheric pressure using a controlled valve (MKS 248D) placed upstream of the pumping system (see figure 1(c)). Here, the applied voltage is synchronized with the pulsed gas injection using the Transistor-Transistor-Logic (TTL) output of the injection control unit.

To determine the total amount of gas injected per pulse, the chamber pressure (P_C) is recorded without the continuous gas flow, and the inlet valve of the pumping system closed (see figure 1(a)). The corresponding pressure rise after each pulse is shown in figure 2(a) for different gas opening time values and upstream pressure values.

As shown in figure 2(a), the pressure rise increases linearly with the gas opening time. In addition, the rate of increase is steeper for the large upstream pressures due to the largest pressure gradient between the pulse injector and the chamber. Based on these results, the instantaneous gas flow Q during each pulse can be defined as

$$Q\left(\mathrm{L\,s^{-1}}\right) = A\frac{\Delta p\ (\mathrm{mbar})}{t_{gas}\ (\mathrm{s})} \qquad (1)$$

where Δp and t_{gas} are the pressure variation and the gas opening time, respectively. By recording the pressure rise as a function of time inside the closed chamber with a known continuous gas flow, a calibration curve (not shown) can be obtained to find the constant A (L $mbar^{-1}$). The corresponding instantaneous gas flow for each pulse is presented in figure 2(b) for various gas opening times and upstream pressures. For a fixed P_U, figure 2(b) shows that Q remains constant regardless of the gas opening time: this confirms that the quantity of gas injected during the gas opening time only depends on the upstream pressure. For the short gas opening times (5 ms and below), the opening and closing times of the valve inside the injection control unit become comparable to the injection time. Hence, in such cases, slightly lower Q values are observed in figure 2(b).

OES measurements are realized using an optical fiber with the tip placed along the middle portion of the discharge.

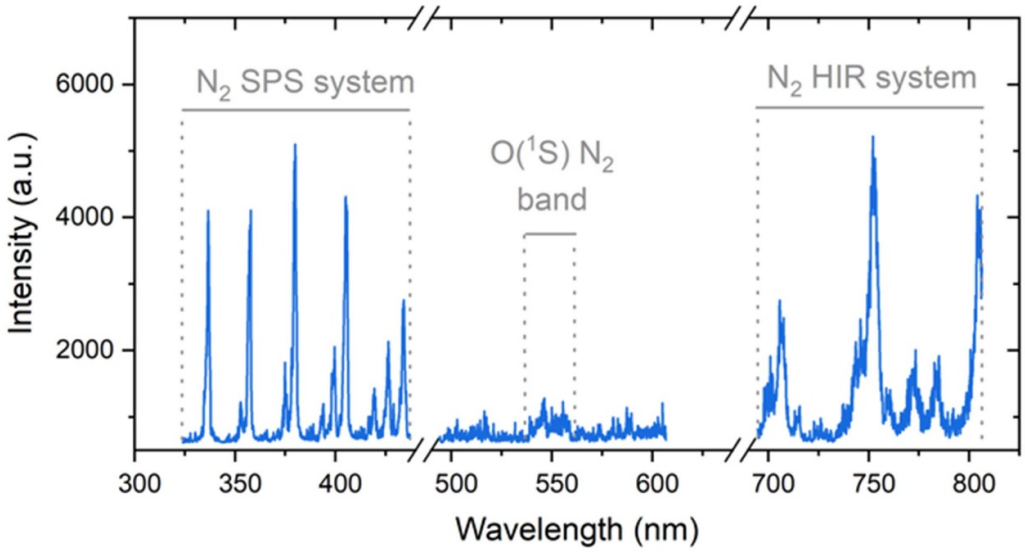

Figure 3. Typical optical emission spectrum of a Townsend discharge in a continuous nitrogen flow.

The signal is transferred to a high-resolution monochromator (Acton SP-2500) equipped with an intensified charged coupled device (iCCD) camera (Princeton Instruments PI-MAX3). OES measurements are synchronized with the pulse injections using the TTL output of the injection control unit. A typical OES spectrum of the Townsend discharge in N_2 at atmospheric pressure is displayed in figure 3 (same conditions as in figure 1(b)).

As can be seen in figure 3, discharge emission is dominated by the Second Positive System (SPS) of N_2, the Herman Infrared system (HIR) of N_2, and the $O(^1S)N_2$ band. Here, the excited $N_2(C)$, $N_2(C'')$, and $O(^1S)N_2$ states giving rise to the observed emission bands are mostly populated according to the following reaction schemes [43–45]:

$$N_2(X) + e^- \rightarrow N_2(C) + e^- \tag{2}$$

$$N_2(A) + N_2(A) \rightarrow N_2(C'') + N_2(X) \tag{3}$$

$$\begin{cases} O(^3P) + N_2(A) \rightarrow O(^1S) + N_2(X) \\ O(^1S) + 2N_2(X) \rightarrow O(^1S)N_2 + N_2(X) \end{cases} \tag{4}$$

Based on equations (2) and (3), the emission intensity of the SPS is typically linked to the electron population [46], whereas the emission intensity of the HIR is ascribed to the square of the population of metastable $N_2(A)$ states [47]. As for the $O(^1S)N_2$ excimer emission, equation (4) reveals that it can be related to both $N_2(A)$ and oxygen impurities [43–45]. In presence of low oxygen concentrations into Townsend N_2 discharges, it is worth highlighting that Lin *et al* [48] have recently shown that associative ionization reaction $N\left(^2P\right) + O\left(^3P\right) \rightarrow NO^+ + e^-$ can be the dominant process involved in the memory effect.

3. Electrical characterization of the discharge

3.1. Townsend discharge with a single pulsed gas injection

Current–voltage characteristics are used to analyze Townsend discharge with a single pulsed gas injection; figure 4(a) to figure 4(c) report the absolute value of the maximum current at each half period of the applied voltage for the entrance, middle, and exit zones of the DBD cell. The results are shown at two gas opening times (10 ms, figure 4(b) and 100 ms, figure 4(c)) for $P_U = 2$ bar. For all experiments, the controlled valve of the pumping system is fixed to $P_C = 1$ bar to maintain atmospheric-pressure conditions in the DBD cell with pulsed gas injections. Values without pulsed gas injections (continuous gas flow only, figure 4(a)) are also presented. For all conditions, the discharge current is very low (<0.5 mA); as reported in the literature [39], this is due to the ionization level not being high enough, which agrees with the behavior of the Townsend discharge in N_2. Furthermore, the maximum current at the entrance of the DBD cell is systematically lower than in the two other zones. A similar feature for continuous gas flows was reported by other authors [36, 43, 48]. In such conditions, the discharge first ignites at the exit, and the population of long-lived metastable $N_2(A)$ states rises between the entrance and the exit; this leads to a lower breakdown voltage and thus to a higher discharge current for the same amplitude of the applied voltage near the exit [43].

Figure 4(a) further shows that regardless of the position along the gas flow lines, the absolute value of the maximum current without pulse (continuous gas flow only) remains constant over time. On one hand, for $t_{gas} = 10$ ms, i.e. for pulse durations shorter than the residence time of the continuous gas flow (~50 ms), figure 4(b) indicates that the maximum current oscillates after the pulsed gas injection up to about 100 ms and then stabilizes. This applies particularly at the

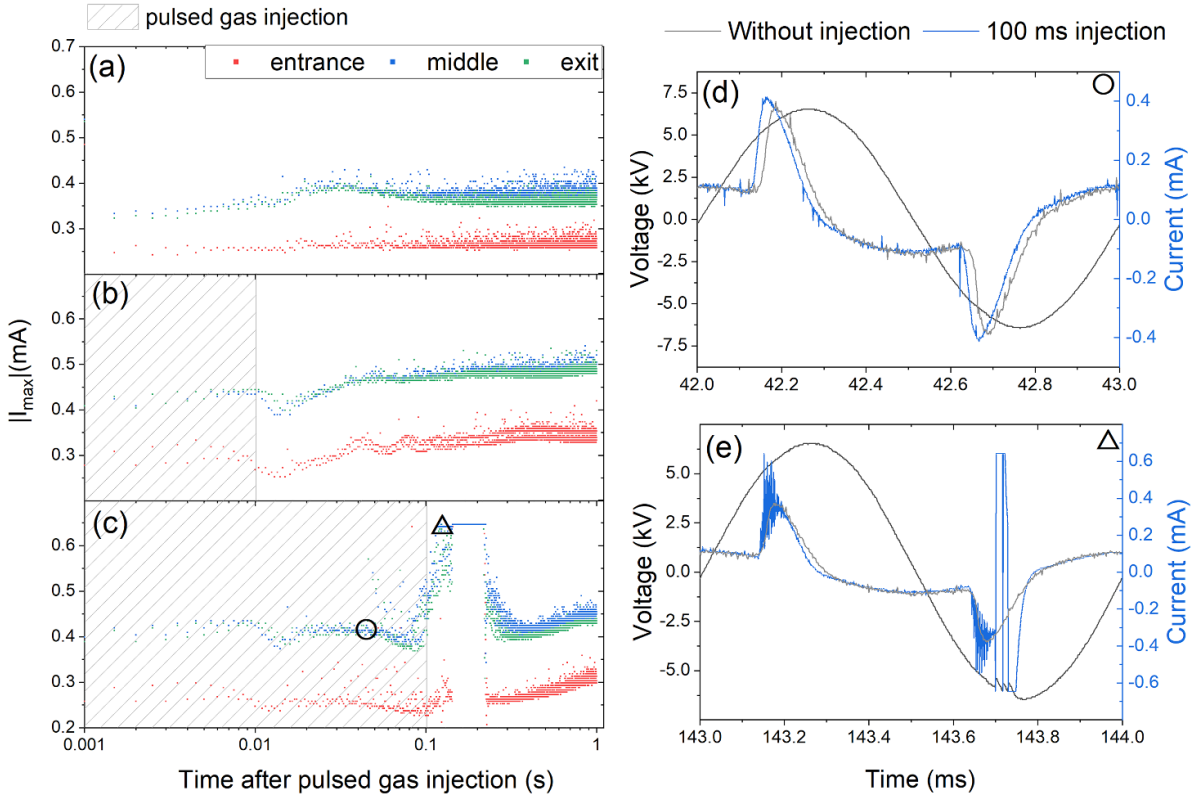

Figure 4. Absolute value of the maximum current at the entrance, middle and exit positions for each half-period of the applied voltage: (a) without pulsed gas injection (continuous gas flow only), (b) with a pulsed gas injection for a pulse duration of 10 ms, and (c) with a pulsed gas injection for a pulse duration of 100 ms. Selected current–voltage characteristics for 100 ms injection: (d) homogeneous Townsend discharge at 0.042 s (◯) and (d) filamentary discharge at 0.143 s (△). Here, the upstream pressure on the injection control unit is fixed to 2 bar.

entrance position, where the memory effect is weaker [43]. On the other hand, for longer pulse durations (for example, t_{gas} = 100 ms), figure 4(c) reveals that the maximum current sharply increases after the pulse end and then oscillates before progressively returning to steady-state values. Such current variation for a pulse duration of 100 ms is linked to the formation of micro-discharges and a temporary transition from the homogeneous to filamentary discharge regime [38]. This can be confirmed by the set of current–voltage characteristics presented in figures 4(d) and (e) for t_{gas} = 100 ms. At 42 ms after the pulsed gas injection, figure 4(d) shows that the discharge remains in the homogenous regime but exhibits a small rise in the breakdown voltage and a slight decrease of the maximum current with respect to the ones observed for continuous gas flow only. In contrast, at 143 ms after the pulsed gas injection, figure 4(e) reveals that the discharge transits to a filamentary regime characterized by narrow discharge channels randomly distributed in time and space [40]. In such conditions, the maximum current significantly varies over very short time scales and can even reach the saturation limit of the oscilloscope.

Discharge destabilization can also be analyzed from the time evolution of the power absorbed or dissipated by electrons in the discharge. Directly obtained from current–voltage characteristics in homogenous discharges [49], the results are presented in figure 5 for several gas opening times (2, 10, 50 and 100 ms) for P_U = 2 bar. Here, all discharge power measurements are collected on the middle electrode (similar features with different values are observed for the entrance and exit zones [36]). While the discharge power remains constant for continuous gas flows in agreement with the evolution of the absolute value of the maximum current (figure 4(a)), two features can be seen in figure 5 for pulsed gas flows: (a) the power remains almost constant up to 10 ms after the beginning of the pulse and then (b) depending on the gas opening time, the power in the homogeneous regime decreases down to the discharge power with only a continuous gas injection and a transition towards the filamentary regime may occur (figures 5(c) and (d)) for the longer durations (50 and 100 ms).

For P_U = 2 bar, the instantaneous gas flow was estimated to 32 l min^{-1} regardless of the gas opening time (see figure 2). Considering the dimensions of the inlet tube, assuming that the gas flow is identical at the outlet of the pulsed injector and throughout the whole system, the pulsed gas can be expected to reach the DBD cell after around 10 ms. Hence, the slight drop in power observed around 10 ms for all conditions can be linked to the sudden arrival of the pulsed gas in the discharge zone. Such a decrease of the discharge power is consistent with a reduction of the discharge current observed over selected time frames in figure 4(d). For 2 ms (figure 5(a)) and 10 ms (figure 5(b)), the pulse duration and the total amount of gas injected per pulse are such that the discharge remains

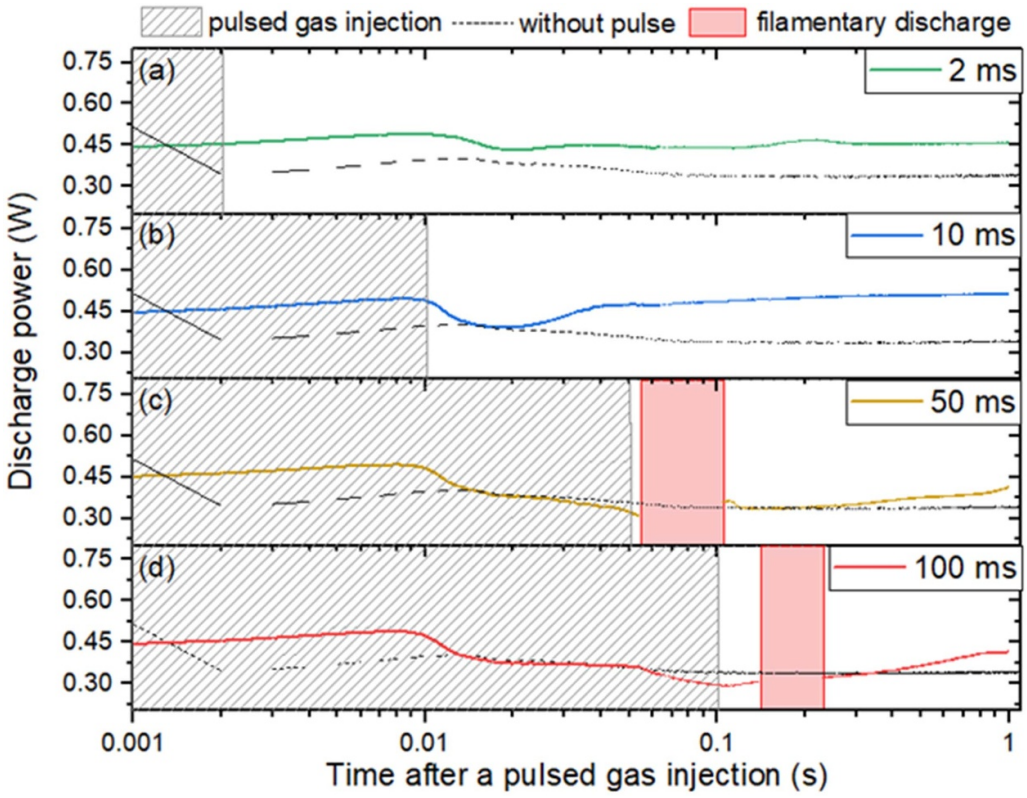

Figure 5. Discharge power (collected on the middle electrode) for various t_{gas}: (a) 2 ms, (b) 10 ms, (c) 50 ms and (d) 100 ms. Here, P_U is fixed to 2 bar. In the red zones, due to oscilloscope saturation in the filamentary regime, the power cannot adequately be calculated from current–voltage characteristics. A small drop is always observed for the first data point (only a few discharges in the 1–2 ms time scale); such a feature can be linked to the transition from filamentary to homogeneous discharge regime due to the time required for the buildup of the memory effect [41, 43].

in the homogeneous regime. For injections over longer time scales (50 ms, see figure 5(c), and 100 ms, figure 5(d)) and thus for larger amounts of gas injected per pulse, however, the discharge becomes filamentary over selected time frames. For example, for 50 and 100 ms gas opening times, this occurs for about 50 and 100 ms, respectively.

3.2. *Townsend discharge with multiple pulsed gas injections*

Based on the data displayed in figure 5, it seems that for single-pulse injections of N_2, the transition from homogeneous to filamentary discharge only occurs when the pulse durations become comparable to the residence time of the continuous gas flow (∼50 ms). However, based on the results presented in figure 2, such a trend with the pulsed gas opening time could also be linked to the total amount of gas injected per pulse. Hence, for longer pulse durations, it seems that the gas from the pulsed injection could no longer be entirely evacuated over the time scale of the continuous gas flow, suggesting a rise in the population of gaseous species. This aspect can be further examined by 'multiple' pulsed injection experiments realized in the specific case of five injections with a gas opening time of 10 ms and $P_U = 2$ bar; the results for the discharge power as a function of time are displayed in figure 6. For the specific set of injection conditions presented in figure 6, the discharge modification becomes more prominent for successive pulsed gas injections, suggesting an accumulation effect from one pulse to the other. More specifically, the decrease of the discharge power after each pulse rises with the number of pulses such that the discharge transits from the homogeneous to the filamentary regime after several pulsed gas injections.

Based on the results in figure 6, discharge destabilization should be more prominent for larger amounts of gas injected per pulse for a given value of t_{gas}. This aspect can be examined by plotting the discharge power variation over time for several values of the upstream pressure P_U, i.e. for different instantaneous flows of the pulsed gas injection (see figure 2); the results are reported in figure 7.

Figure 7 reveals that the slight drop in discharge power linked to the sudden arrival of the pulsed gas occurs earlier at 2.5 bar (∼80 ms) than at 1.5 bar (∼130 ms). Based on the results presented in figure 2, such behavior is consistent with the corresponding rise in the instantaneous pulsed gas flow for $t_{gas} = 10$ ms, going from about 24 l min^{-1} at 1.5 bar to about 41 l min^{-1} at 2 bar. Figure 7 also shows that the extent of the discharge destabilization rises with P_U. More specifically, while the discharge remains in the homogeneous regime up to at least five pulses for $P_U = 1.5$ bar (figure 7(a)), the discharge destabilization intensifies with the number of pulses for $P_U = 2.5$ bar (figure 7(b)). Such behavior is very good

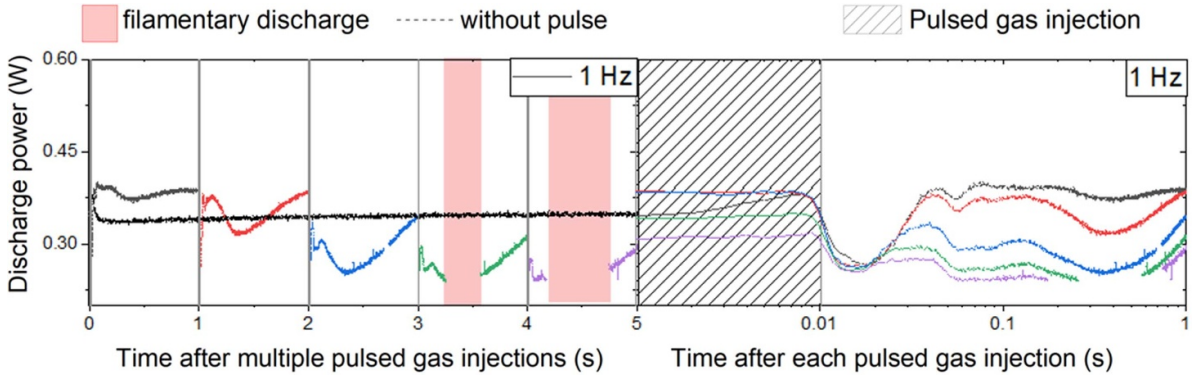

Figure 6. Discharge power for t_{gas}= 10 ms, 2 bar. The data are plotted over two-time scales: on a linear scale after multiple pulsed gas injections (left) and on a log scale after each pulsed gas injection (right). The same colour code is used in both cases: black-first pulse, red-second pulse, blue-third pulse, green-fourth pulse and purple-fifth pulse.

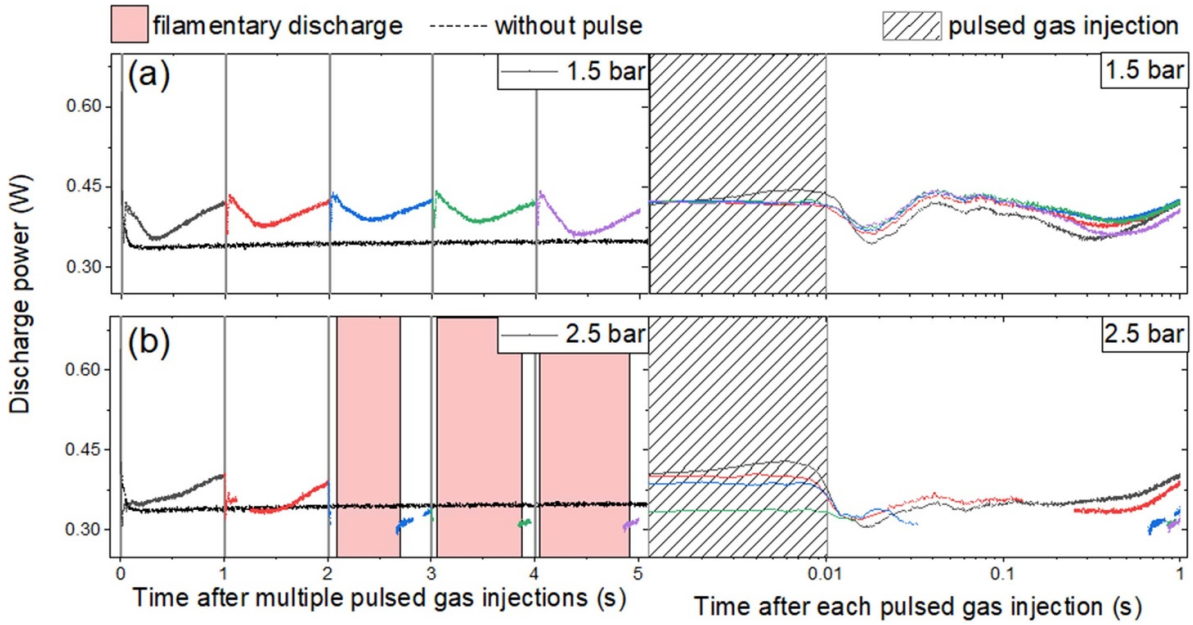

Figure 7. Discharge power for t_{gas} = 10 ms and several upstream pressure values: (a) 1.5 and (b) 2.5 bar. The data are plotted over two-time scales: on a linear scale after multiple pulsed gas injections (left) and on a log scale after each pulsed gas injection (right). The same color code is used in both cases: black-first pulse, red-second pulse, blue-third pulse, green-fourth pulse and purple-fifth pulse.

agreement with a cumulative effect of the pulsed gas injection on the stability of Townsend discharge. Discharge modification is more prominent for larger amounts of gas injected per pulse, and thus for longer pulses at fixed instantaneous pulsed gas flows (figure 5) or higher instantaneous pulsed gas flows at fixed pulsed duration (figure 7). Of note, it can be seen from the set of data presented in figures 6 and 7 that the transition from the homogeneous to the filamentary discharge regime occurs when the discharge power reaches a critical value around 0.3 W.

A similar cumulative effect can be seen by varying the pulsed injection frequency for t_{gas} = 10 ms and P_U = 2 bar (figure 8). After the first pulse, the same decrease of the discharge power at 10 ms is observed for 0.1 Hz (figure 8(a)), 1 Hz (figure 6), and 10 Hz (figure 8(b)); this trend is consistent with the fixed value of the instantaneous pulsed gas flow (32 l min^{-1}, figure 2). After such a temporary drop, the discharge power increases back to the value achieved without any pulsed gas injection. Depending on the injection frequency, two distinct trends can be seen: (a) if the injection period ($1/f$) is long enough to retrieve power values higher than the critical one, the discharge will remain or go back to a homogeneous discharge regime, and (b) if not enough time is provided to the discharge before a subsequent pulse, the power does not increase back to the critical value and the discharge will remain filamentary.

As mentioned previously, through selective control of the operating conditions, N_2 discharges can be homogeneous due to the presence of long-lived species from one half-cycle of the applied voltage to the other. Involved in the production of seed electrons at low electric fields [41, 43], any factor leading to a net loss of metastable $N_2(A)$ states would no longer ensure

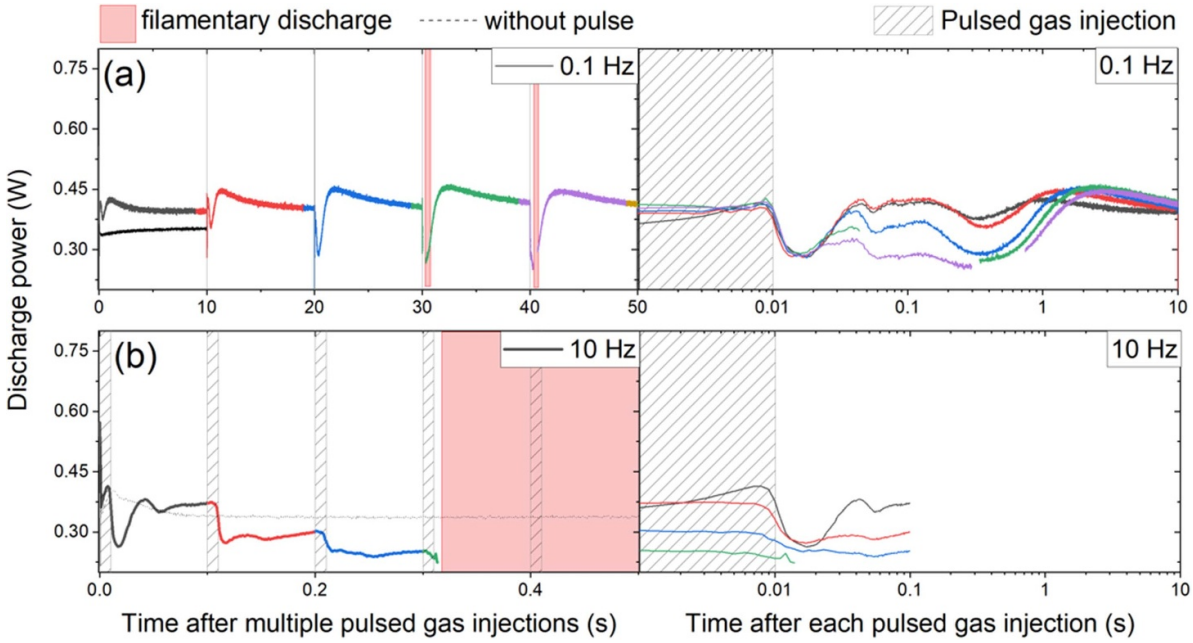

Figure 8. Discharge power for $t_{gas} = 10$ ms at (a) 0.1 Hz and (b) 10 Hz injection frequency. The data are plotted over two-time scales: on a linear scale after multiple pulsed gas injections (left) and on a log scale after each pulsed gas injection (right). The same color code is used in both cases: black-first pulse, red-second pulse, blue-third pulse, green-fourth pulse and purple-fifth pulse.

conditions for homogeneous discharge formation [21]. Hence, the Townsend breakdown would be replaced by a streamer breakdown, and the discharge would transit to a filamentary regime. This is typically accompanied by an increase in the breakdown voltage [21]; this feature is consistent with the data presented in figure 4(d). One of the phenomena leading to a net metastable loss in N_2 discharges is the quenching of $N_2(A)$ states by gas-phase collisions [21]. Hence, additional gas-phase species arising from the pulsed gas injections and the cumulative effect can play an important role on the populations of $N_2(A)$ states and, thus on the stability of Townsend discharges. In particular, the set of current–voltage characteristics for single and multiple injections have shown that gas accumulation can be linked to many possible routes: (a) pulse durations longer than the residence time of the continuous gas flow at fixed instantaneous pulsed gas flows, (b) larger instantaneous pulsed gas flows at fixed pulsed duration, and (c) multiple pulsed injections with repetition frequencies between 0.1 and 10 Hz. In line with this discussion, any significant change of the neutral gas composition, for example, in the presence of impurities or precursors used for materials processing, could modify the discharge stability; we will return to this point later.

3.3. Optical emission spectroscopy of the discharge

OES is used to examine in more detail the stability of Townsend N_2 discharges with pulsed gas injections. Here, the gas tubes and discharge chamber are flushed more than ten times with nitrogen before the experiment to ensure a minimal contribution from outgassing and thus from impurities emanating from surfaces [50]. In such conditions, it is found that the homogeneous discharge regime can be maintained over a larger number of pulses than in the previous set of less standardized experiments (figures 6–8). Figure 9 presents the time evolution of the discharge power and selected emission intensities for ten pulsed gas injections. Here, the gas opening time, upstream pressure, and injection frequency are fixed to 10 ms, 2 bar, and 1 Hz, respectively. Values for a Townsend discharge with a continuous flow of nitrogen are also shown for comparison.

As highlighted in the previous section, figure 9(a) indicates that the discharge power decreases sharply with the pulsed gas injection but returns to a pre-defined value after each perturbation. After several injections, however, the power continues to decrease without returning to the value before perturbation. A similar trend is observed in figure 9(b) for the emission intensity of the SPS of N_2 linked to the $N_2(C)$ state [44]. From equation (1), $N_2(C)$ is mainly populated by electron-impact collisions on ground state $N_2(X)$. Therefore, the similar trend in the time evolution of the discharge power and N_2 SPS emission intensity over time can partially be linked to temporal variations of the electron density (linked to the discharge power). In this framework, the $N_2(C)$ emission intensity is divided by the discharge power to analyze the time evolution of $N_2(X)$ with pulsed gas injection; the results are presented in figure 9(e). While no significant change can be seen for the first few pulses, a slight decrease occurs following each additional pulse with an accumulative effect for a larger number of pulses. It is important to note that additional gas or any change in the gas composition can induce temporal modification of the collisional quenching of emitting $N_2(C)$ states [21, 51]: hence, the behavior observed in figure 9(e) can result from time variations of both $N_2(X)$ and optical efficiency of $N_2(C)$-to-$N_2(B)$

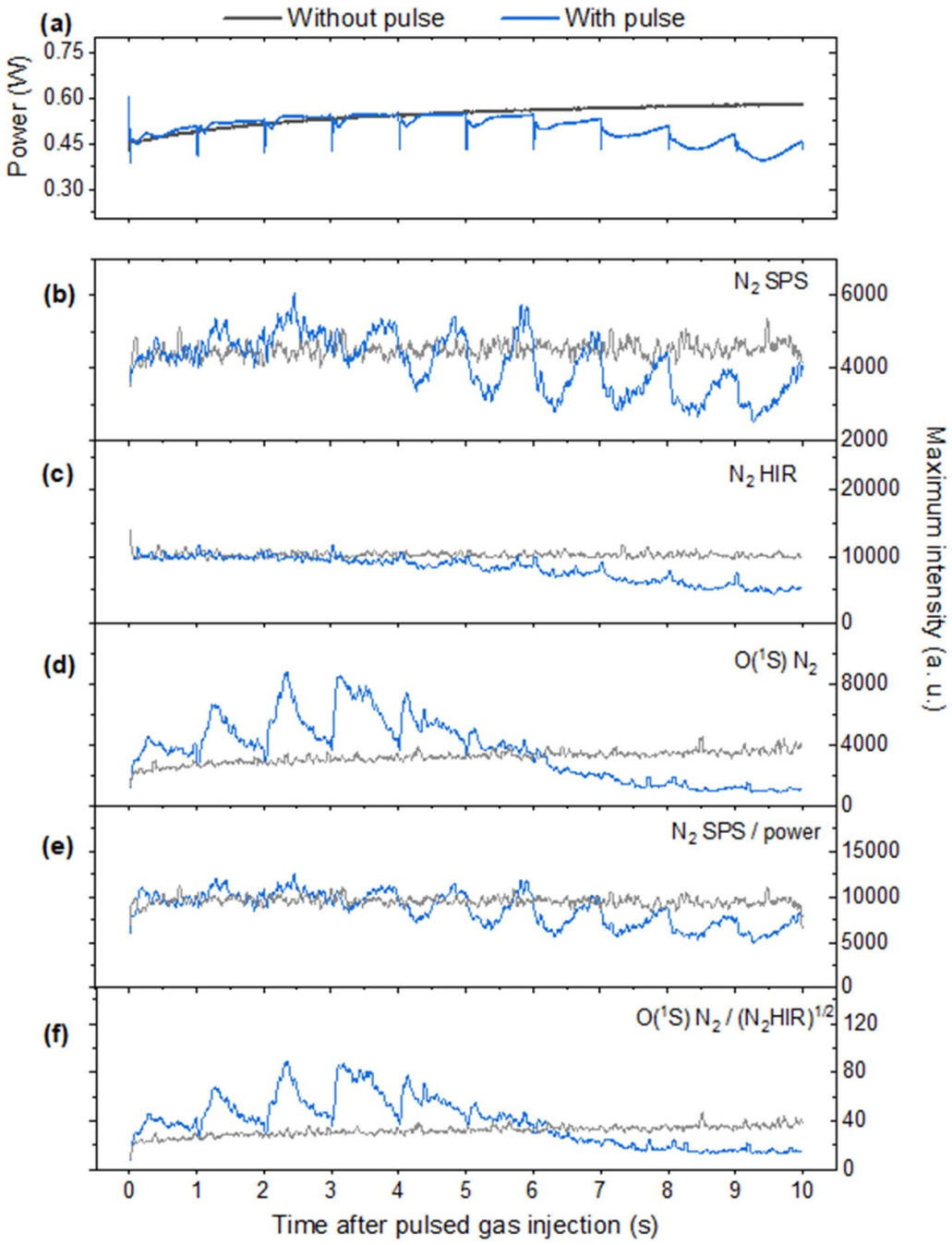

Figure 9. (a) Discharge power with and without gas injection. Evolution of the emission intensity of (b) N_2 SPS, (c) N_2 HIR, (d) $O(^1S)N_2$, (e) N_2 SPS/Power and (f) $O(^1S)N_2/(N_2HIR)^{0.5}$. Here, the gas opening time, upstream pressure, and injection frequency are fixed to 10 ms, 2 bar, and 1 Hz, respectively.

transitions (due, for example, to the incorporation of impurities, see below).

As for the N_2 HIR emission (see figure 9(c)), it monotonously decreases with time. For a large number of pulses, a decrease can also be seen on the time frame of each single pulse. Based on equation (2), such short and long-time scale diminutions are a signature of $N_2(A)$ losses [44]. In figure 9(d), the time evolution of the emission intensity from the $O(^1S)$ N_2 system presents two features. First, between the first and the fourth injection, the emission intensity globally increases with a return to the pre-defined value before the next pulse. Based on equation (3), two parameters can result in an increase in $O(^1S)N_2$ emission: (a) an increase of the population of $N_2(A)$ states and (b) an increase in the population of oxygen $O(^3P)$ state [44, 45]. Since the emission intensity of N_2 HIR linked to the population of $N_2(A)$ either remains either constant or shows the opposite trend in the first 4 s of the experiment (figure 9(c)), the increase in $O(^1S)N_2$ most likely arises from an increase in the number density of oxygen atoms. This can be confirmed in figure 9(f) by the ratio of the emission intensity

of $O(^1S)$ N_2 over the square root of the emission intensity of the N_2 HIR system; this ratio is directly linked to the evolution of oxygen species. Second, after the fifth pulse, the emission intensity decreases drastically for both N_2 HIR and $O(^1S)N_2$; such trend can be explained by the net loss of $N_2(A)$ due to the expected quenching by oxygen species [37].

Through a more detailed look at a single pulsed injection (over 1 s), it can be noticed in figures 9(e) and (f) that the rate of change in $N_2(X)$ (and/or optical efficiency) and $O(^3P)$ populations is very slow considering the expected residence time of gas-phase species in the DBD cell. With an instantaneous gas flow around 32 l min^{-1} (see figure 2), the corresponding gas residence time can be estimated to 2 ms. In addition to the pulsed gas injections, there is a continuous flow of nitrogen characterized by a residence time of about 50 ms. As can be seen in figure 9, the more prominent variations of the $N_2(X)$ (and/or optical efficiency) and $O(^3P)$ populations occur halfway along the gas injection period, i.e. 0.5 s. This result suggests other mechanisms occurring over much longer time scales than those linked to continuous and pulsed nitrogen gas flows.

4. Discussion

Further characterization of the pulsed gas flow channel can be realized using the set of data presented in figure 2. As can be seen in figure 10, regardless of the gas opening time, the instantaneous gas flow, Q, increases with the pressure difference between the upstream and the chamber pressures, P_U–P_C (P_C being set to atmospheric pressure). In the case of a linear variation (Hagen–Poiseuille equation in a laminar gas flow [52]), the proportionality constant corresponds to the so-called fluid conductance. However, the significant departure from the linear trend displayed in figure 10 suggests that the Hagen–Poiseuille equation is not suitable. Two hypotheses can be made to interpret this non-linearity, either a transition from laminar to turbulent gas flow or the head losses due to the specific gas flow channel [52].

To analyze the possible transition from laminar to turbulent gas flow, the Reynolds number, $Re = \frac{\rho.U.D}{\mu}$, where ρ is the gas mass density, U is the gas average velocity, D is the characteristic dimension of the system, and μ is the dynamic viscosity, was calculated. Over the range of experimental conditions investigated, Re rises from about 35 for the continuous gas flow of 1 l min^{-1} to more than 1000 for an instantaneous gas flow of 32 l min^{-1}; this result is consistent with an instantaneous transition from laminar to an intermediate flow regime over the time scale of the pulsed gas injection [52]. However, filamentation appears on time scales much longer than the pulse duration and not necessarily after the first injection. Furthermore, the extent of discharge destabilization varies with the injection frequency. Since these aspects are unrelated to Reynold's number and thus to a change in the gas flow regime, other issues must be involved, most likely singular head losses due to irregularities from the inlet pipe to the gas mixing chamber and then to the DBD cell (see figure 1).

To understand the pulsed gas injection behavior over the range of experimental conditions investigated, 2D simulations are done using COMSOL Multiphysics [53] Here, simulations are performed along the discharge axis, with the mixing chamber allowing a coupling between the inlet gas pipes (continuous and pulsed gas flows) and the DBD cell (see figure 1). The injection conditions simulated by COMSOL are as determined experimentally, i.e. a continuous flow rate of 1 l min^{-1} and a pulsed injection of 10 ms at 0.1 Hz (instantaneous flow rate of 32 l min^{-1}). To prevent sharp transitions in numerical analysis, the pulse is simulated with a rise time of 5 ms, a plateau of 10 ms, and a decay time of 50 ms. Figure 11(a) shows the time-resolved gas velocity calculated at the center of the interelectrode gap. As expected, the gas velocity sharply rises and then drastically decreases after each pulsed injection. No accumulation can be seen from one pulse to the other. Hence, the gas flow in the DBD cell does not seem to be modified out of the time scale of the instantaneous pulsed gas flow.

Figures 11(b)–(d) show 2D mappings of the gas velocity before the fourth 10 ms pulse ((b), Time 1 (3.09 s) in (a)), after the fourth 10 ms pulse ((c), Time 2 (3.11 s) in (a)), and 1 ms after the fourth 10 ms pulse ((d), Time 3 (3.20 s) in (a)). In all cases, the gas velocity profile with respect to height in the interelectrode space remains nearly parabolic. This behavior is consistent with the low Womersley number (from 0.2 to 2 between 0.1 and 10 Hz). In such conditions, the frequency of pulsations is sufficiently low that a parabolic velocity profile (Hagen–Poiseuille equation [52]) has time to develop during each cycle, and the flow remains nearly in phase with the instantaneous pressure gradient [54]. However, it can be seen in figures 11(b)–(d) that pulsed gas injection introduces recirculations in the gas mixing chamber located upstream of the DBD cell. In addition, these recirculations remain from one pulse to the other (for example, from the end of one pulse shown in figure 11(d) to the onset of another pulse as in figure 11(b)). Hence, due to the longer gas residence time in the mixing chamber, impurities inherently outgassing from chamber walls can accumulate in this region of the reactor, and then be released at abnormally high concentrations in the DBD cell.

This possible change in the neutral gas composition is considered by introducing in COMSOL simulations a constant oxygen desorption rate from the walls of the mixing chamber. Here the flux is estimated to 10^{-5} mol m^{-2} s^{-1} to produce an oxygen molar fraction in the discharge zone of a few ppm. Figure 12(a) reveals that such feature introduces significant temporal variation of the relative oxygen content. Clearly, a sudden rise in the oxygen molar fraction occurs after each pulse, with a shape similar to the one of the gas velocity. However, while the gas velocity linked to the pulsed injection rapidly returns to the value of the continuous gas flow, a second rise in the oxygen content with much slower decay occurs between each pulse. An accumulation from the first pulse to the others with a steady-state concentration value for longer number of pulses can also be seen. As highlighted in figures 12(b)–(d), such variations characterized by much longer time scales than those linked to pulsed and continuous

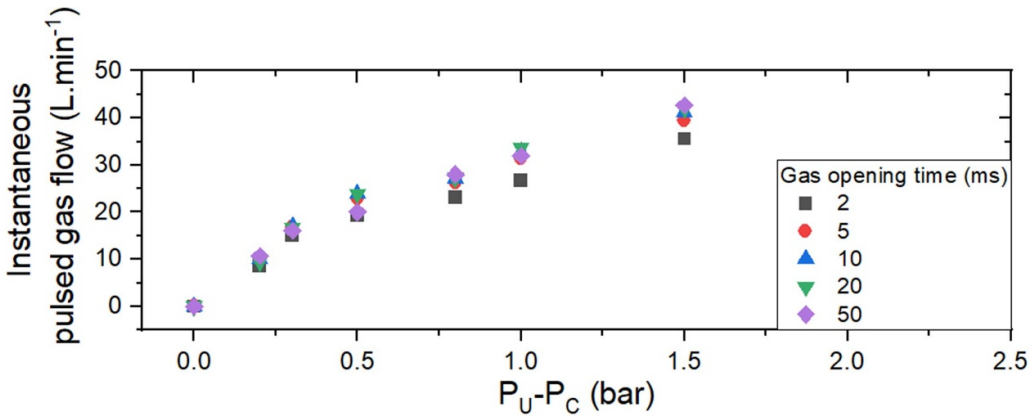

Figure 10. Correlation between the instantaneous pulsed gas flow Q and the pressure difference between the pulse injector and the chamber P_U–P_C for various gas opening times.

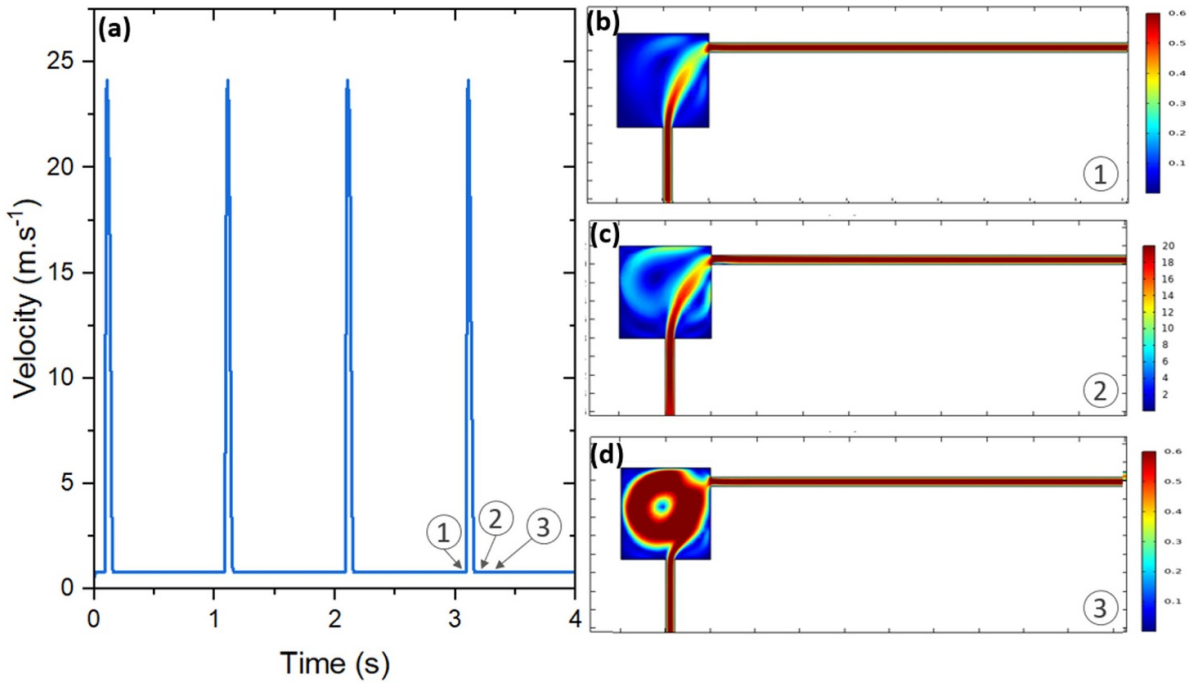

Figure 11. (a) Gas velocity profile obtained from COMSOL simulations at the centre of the inter-electrodes space. 2D mapping of the gas flow lines at (b) 3.09 (Time 1, before the 10 ms pulse), (c) 3.11 (Time 2, after the 10 ms pulse) and (d) 3.20 s (Time 3, 10 ms after the 10 ms pulse). The injection conditions simulated by Comsol are as follows: a continuous flow rate of 1 l·min^{-1} and a pulsed injection of 10 ms at 0.1 Hz (instantaneous flow rate of 32 l·min^{-1}).

gas flow are directly linked to surface outgassing and recirculations in the gas mixing chamber.

Of note, the behaviors presented in figure 12 are comparable to the one of the O(^{3}P), and the opposite to the one of the N_2(A) observed by time-resolved OES (figure 9). Hence, the incorporation of oxygen impurities through surface outgassing and recirculations in the gas mixing chamber can contribute to N_2(A) losses and thus to a discharge destabilization, in excellent agreement with the experiments for both single pulse and multiple pulses (figures 4, 5, 7 and 8). Several studies have examined the influence of oxygen impurities on the fundamental properties of DBD operated in N_2. For a low amount of oxygen (up to a few tens of ppm), the power rises with the oxygen addition. However, the opposite trend is observed at higher oxygen content [43]. In addition, high oxygen content leads to a transition from the homogeneous to the filamentary discharge regime. This set of results is again consistent with the electrical and optical characteristics presented for single pulse and multiple pulses. It is worth mentioning that the results presented in figure 12 are obtained with an oxygen desorption rate from the walls of 10^{-5} mol m^{-2} s^{-1}, yielding oxygen molar fractions in the discharge zone of a few ppm. Similar trends were observed for other desorption rates: hence, the behavior displayed in figure 12 remains, with a linear rise of the steady-state oxygen molar concentration value with the oxygen desorption rate.

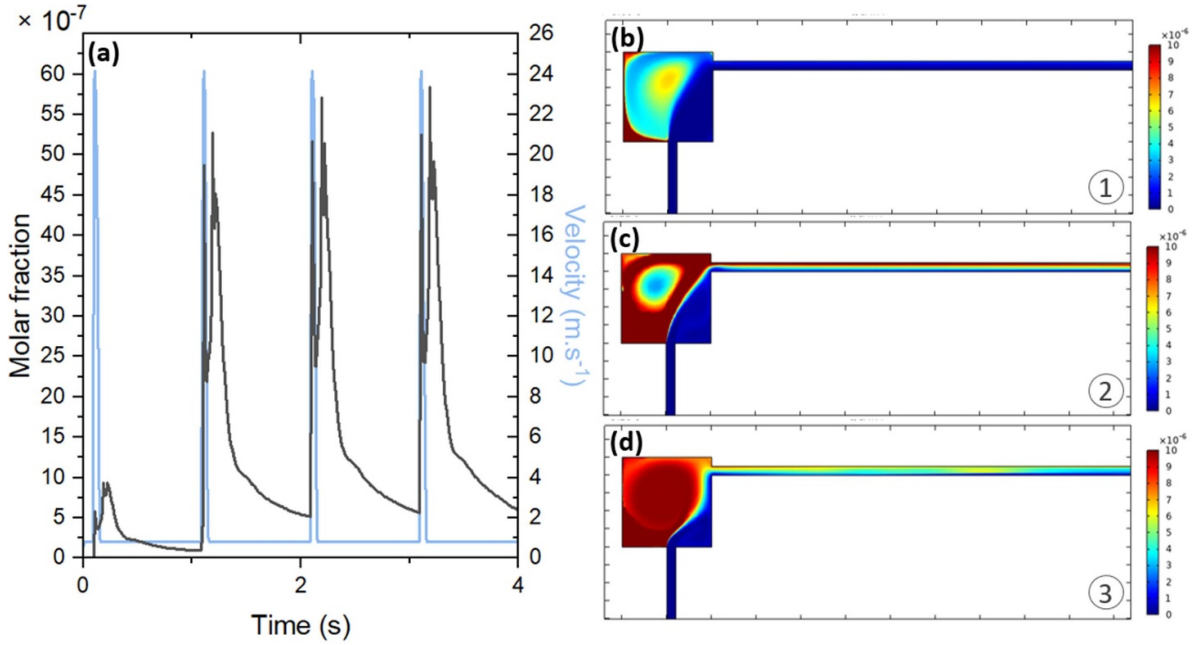

Figure 12. Oxygen molar content obtained from COMSOL simulations at the centre of the inter-electrodes space. 2D mapping of the oxygen content at (b) 3.09 (Time 1, before the 10 ms pulse), (c) 3.11 (Time 2, after the 10 ms pulse) and (d) 3.20 s (Time 3, 10 ms after the 10 ms pulse). The injection conditions simulated by COMSOL are as follows: a continuous flow rate of 1 l min^{-1}, a pulsed injection of 10 ms at 0.1 Hz (instantaneous flow rate of 32 l min^{-1}), and an oxygen desorption rate from the chamber walls of 10^{-5} mol m^{-2} s^{-1}. In (a), the gas velocity is also shown for comparison.

5. Conclusion

The objective of this work was to understand the behavior of Townsend DBD operated in a homogeneous regime following pulsed gas injection. Time-resolved discharge power measurements coupled with OES analysis have been realized over single and multiple pulsed injections of nitrogen in a continuous laminar nitrogen gas flow. The effects on discharge stability of three main pulsed injection parameters have been analyzed: (a) gas opening time (pulse duration), (b) instantaneous pulsed gas flow (through modification of the upstream pressure P_U), and (c) pulse repetition frequency. For single pulsed gas injection, discharge power measurements revealed that gas opening times longer than 50 ms yield to a filamentary discharge regime. For larger amounts of gas injected per pulse and successive pulsed gas injections, transition from homogeneous to filamentary also occurred. In such conditions, OES revealed an increase of nitrogen and oxygen species leading to a significant loss of metastable $N_2(A)$ species and hence of the memory effect, which is essential to obtain a Townsend discharge.

Over the range of experimental conditions investigated characterized by high instantaneous gas flows due to pulsed injection in a continuous gas flow, it was found that surface outgassing and gas recirculations in the gas mixing chamber located upstream of the DBD cell can induce oxygen impurities in the discharge over much longer time scales than the ones expected from the instantaneous and continuous gas flows. However, it can be expected that such features are directly linked to the dimension and shape of the system, in particular of the gas mixing chamber. As will be demonstrated in forthcoming papers, the operation of Townsend discharges in pulsed gas flow regimes show interest for several applications, in particular for the deposition of multifunctional thin films.

Data availability statement

The data that support the findings of this study are available upon reasonable request from the authors.

Acknowledgments

This work was financially supported by the Université Toulouse III—Paul-Sabatier and Direction des Relations Internationales of the Université de Montréal through their contributions to the Québec-France International Research Network on Nanomatériaux Multifonctionnels Contrôlés (IRN-NMC).

ORCID iDs

R Clergereaux https://orcid.org/0000-0001-8014-6154
N Naudé https://orcid.org/0000-0002-8534-4114
L Stafford https://orcid.org/0000-0003-0647-543X

References

[1] Profili J, Levasseur O, Blaisot J-B, Koronai A, Stafford L and Gherardi N 2016 Nebulization of nanocolloidal suspensions for the growth of nanocomposite coatings in dielectric barrier discharges *Plasma Process Polym.* **13** 981–9

[2] Fanelli F, Mastrangelo A M and Fracassi F 2014 Aerosol-assisted atmospheric cold plasma deposition and characterization of superhydrophobic organic–inorganic nanocomposite thin films *Langmuir* **30** 857–65

[3] Biniwale R B, Mizuno A and Ichikawa M 2004 Hydrogen production by reforming of iso-octane using spray-pulsed injection and effect of non-thermal plasma *Appl. Catal.* A **276** 169–77

[4] Kameshima S, Tamura K, Ishibashi Y and Nozaki T 2015 Pulsed dry methane reforming in plasma-enhanced catalytic reaction *Catal. Today* **256** 67–75

[5] Jiménez C *et al* 2007 Deposition of TiO_2 thin films by atmospheric plasma post-discharge assisted injection MOCVD *Surf. Coat. Technol.* **201** 8971–5

[6] Dingemans G, Van De Sanden M C M and Kessels W M M 2012 Plasma-enhanced chemical vapor deposition of aluminum oxide using ultrashort precursor injection pulses *Plasma Process Polym.* **9** 761–71

[7] Sproul W D 1987 High rate reactive sputtering process control *Surf. Coat. Technol.* **33** 73–81

[8] Martin N, Bally A R, Hones P, Sanjines R and Levy F 2000 High rate and process control of reactive sputtering by gas pulsing: the Ti-O system *Thin Solid Films* **377–378** 550–6

[9] Kushner M J 1993 Pulsed plasma-pulsed injection sources for remote plasma activated chemical vapor deposition *J. Appl. Phys.* **73** 4098–100

[10] Kwon S J 2005 Effect of precursor-pulse on properties of Al-doped ZnO films grown by atomic layer deposition *Jpn. J. Appl. Phys.* **44** 1062

[11] Metzler D, Bruce R L, Engelmann S, Joseph E A and Oehrlein G S 2014 Fluorocarbon assisted atomic layer etching of SiO_2 using cyclic Ar/C_4F_8 plasma *J. Vac. Sci. Technol.* A **32** 020603

[12] Groner M D, Elam J W, Fabreguette F H and George S M 2002 Electrical characterization of thin Al_2O_3 films grown by atomic layer deposition on silicon and various metal substrates *Thin Solid Films* **413** 186–97

[13] Pánek R, Gunn J P, Bucalossi J, Ďuran I, Geraud A, Hron M, Loarer T, Pégourié B, Stöckel J and Tsitrone E 2005 The response of the Tore Supra edge plasma to supersonic pulsed gas injection *J. Nucl. Mater.* **337–339** 530–4

[14] Sadek T, Carnide G, Vinchon P, Kahn M L, Clergereaux R and Stafford L 2022 Time-resolved analysis of the electron temperature in RF magnetron discharges with a pulsed gas injection *submitted*

[15] Garofano V, Stafford L, Despax B, Clergereaux R and Makasheva K 2015 Cyclic evolution of the electron temperature and density in dusty low-pressure radio frequency plasmas with pulsed injection of hexamethyldisiloxane *Appl. Phys. Lett.* **107** 183104

[16] Garofano V, Bérard R, Boivin S, Joblin C, Makasheva K and Stafford L 2019 Multi-scale investigation in the frequency domain of Ar/HMDSO dusty plasma with pulsed injection of HMDSO *Plasma Sources Sci. Technol.* **28** 055019

[17] Garofano V, Bérard R, Glad X, Joblin C, Makasheva K and Stafford L 2019 Time-resolved analysis of the precursor fragmentation kinetics in an hybrid PVD/PECVD dusty plasma with pulsed injection of HMDSO *Plasma Process Polym.* **16** 1900044

[18] Fan Z, Qi H, Liu Y, Yan H and Ren C 2016 Effects of airflow on the distribution of filaments in atmospheric AC dielectric barrier discharge *Phys. Plasmas* **23** 123520

[19] Liu F, Zhang D and Wang D 2010 Gas flow effects on the submicrosecond pulsed atmospheric pressure glow discharges *Phys. Plasmas* **17** 103508

[20] Höft H, Becker M M and Kettlitz M 2016 Impact of gas flow rate on breakdown of filamentary dielectric barrier discharges *Phys. Plasmas* **23** 033504

[21] Massines F, Gherardi N, Naudé N and Ségur P 2009 Recent advances in the understanding of homogeneous dielectric barrier discharges *Eur. Phys. J. Appl. Phys.* **47** 22805

[22] Massines F, Sarra-Bournet C, Fanelli F, Naudé N and Gherardi N 2012 Atmospheric pressure low temperature direct plasma technology: status and challenges for thin film deposition *Plasma Process Polym.* **9** 1041–73

[23] Levasseur O, Vlad M, Profili J, Gherardi N, Sarkissian A and Stafford L 2017 Deposition of fluorocarbon groups on wood surfaces using the jet of an atmospheric-pressure dielectric barrier discharge *Wood Sci. Technol.* **51** 1339–52

[24] Profili J, Levasseur O, Koronai A, Stafford L and Gherardi N 2017 Deposition of nanocomposite coatings on wood using cold discharges at atmospheric pressure *Surf. Coat. Technol.* **309** 729–37

[25] de Larclause I S, Paulmier T, Enache I, Caquineau H, Raynaud P, Massines F and Gherardi N 2009 Conformity of silica-like thin films deposited by atmospheric pressure Townsend discharge and transport mechanisms *IEEE Trans. Plasma Sci.* **37** 970–8

[26] Cote D R, Nguyen S V, Stamper A K, Armbrust D S, Tobben D, Conti R A and Lee G Y 1999 Plasma-assisted chemical vapor deposition of dielectric thin films for ULSI semiconductor circuits *IBM J. Res. Dev.* **43** 5–38

[27] Avasthi D K, Mishra Y K, Kabiraj D, Lalla N P and Pivin J C 2007 Synthesis of metal—polymer nanocomposite for optical applications *Nanotechnology* **18** 125604

[28] Levasseur O, Stafford L, Gherardi N, Naudé N, Blanchard V, Blanchet P, Riedl B and Sarkissian A 2012 Deposition of hydrophobic functional groups on wood surfaces using atmospheric-pressure dielectric barrier discharge in helium-hexamethyldisiloxane gas mixtures *Plasma Process Polym.* **9** 1168–75

[29] Massines F, Gherardi N, Fornelli A and Martin S 2005 Atmospheric pressure plasma deposition of thin films by Townsend dielectric barrier discharge *Surf. Coat. Technol.* **200** 1855–61

[30] Martin S 2004 Atmospheric pressure PE-CVD of silicon based coatings using a glow dielectric barrier discharge *Surf. Coat. Technol.* **177–178** 693–8

[31] Profili J, Levasseur O, Naudé N, Chaneac C, Stafford L and Gherardi N 2016 Influence of the voltage waveform during nanocomposite layer deposition by aerosol-assisted atmospheric pressure Townsend discharge *J. Appl. Phys.* **120** 053302

[32] Profili J, Rousselot S, Tomassi E, Briqueleur E, Aymé-Perrot D, Stafford L and Dollé M 2020 Toward more sustainable rechargeable aqueous batteries using plasma-treated cellulose-based Li-Ion electrodes *ACS Sustain. Chem. Eng.* **8** 4728–33

[33] Durán I R, Profili J, Stafford L and Laroche G 2020 Beyond microelectronics with 1,3,5,7-tetramethylcyclotetrasiloxane: a promising molecule for anti-fogging coatings *Mater Chem. Phys.* **242** 122508

[34] Prégent J, Vandsburger L, Blanchard V, Blanchet P, Riedl B, Sarkissian A and Stafford L 2015 Modification of hardwood samples in the flowing afterglow of N_2–O_2 dielectric barrier discharges open to ambient air *Cellulose* **22** 3397–408

[35] Prégent J, Vandsburger L, Blanchard V, Blanchet P, Riedl B, Sarkissian A and Stafford L 2015 Determination of active species in the modification of hardwood samples in the flowing afterglow of N_2 dielectric barrier discharges open to ambient air *Cellulose* **22** 811–27

[36] Mejanes N D, Profili J, Babaei S, Naudé N and Stafford L 2021 Refined analysis of current–voltage characteristics in Townsend dielectric barrier discharges in nitrogen at atmospheric pressure *J. Appl. Phys.* **54** 095204
[37] Gherardi N and Massines F 2001 Mechanisms controlling the transition from glow silent discharge to streamer discharge in nitrogen *IEEE Trans. Plasma Sci.* **29** 536–44
[38] Naudé N, Cambronne J-P, Gherardi N and Massines F 2005 Electrical model and analysis of the transition from an atmospheric pressure Townsend discharge to a filamentary discharge *J. Phys. D: Appl. Phys.* **38** 530–8
[39] Massines F, Gherardi N, Naudé N and Ségur P 2005 Glow and Townsend dielectric barrier discharge in various atmosphere *IPP Plasma Phys. Control. Fusion* **47** B577
[40] Kogelschatz U 2002 Filamentary, patterned, and diffuse barrier discharges *IEEE Trans. Plasma Sci.* **30** 1400–8
[41] Gherardi N, Gouda G, Gat E, Ricard A and Massines F 2000 Transition from glow silent discharge to micro-discharges in nitrogen gas *Plasma Sources Sci. Technol.* **9** 340–6
[42] Bosan D A, Jovanovic T V and Krmpotic D M 1997 The role of neutral metastable molecules in the breakdown probability and glow discharge in nitrogen *J. Phys. D: Appl. Phys.* **30** 3096–8
[43] Tyl C, Lin X, Bouzidi M C, Dap S, Caquineau H, Ségur P, Gherardi N and Naudé N 2018 Investigation of memory effect in atmospheric pressure dielectric barrier discharge in nitrogen with small oxygen or nitric oxide addition *J. Phys. D: Appl. Phys.* **51** 354001
[44] Kossyi I A, Kostinsky A Y, Matveyev A A and Silakov V P 1992 Kinetic scheme of the non-equilibrium discharge in nitrogen-oxygen mixtures *Plasma Sources Sci. Technol.* **1** 207–20
[45] Brandenburg R, Maiorov V A, Golubovskii Y B, Wagner H-E, Behnke J and Behnke J F 2005 Diffuse barrier discharges in nitrogen with small admixtures of oxygen: discharge mechanism and transition to the filamentary regime *J. Phys. D: Appl. Phys.* **38** 2187–97
[46] Kogelheide F, Offerhaus B, Bibinov N, Krajinski P, Schücke L, Schulze J, Stapelmann K and Awakowicz P 2020 Characterisation of volume and surface dielectric barrier discharges in N_2–O_2 mixtures using optical emission spectroscopy *Plasma Process Polym.* **17** 1900126
[47] Simek M, Babický V, Clupek M and Sunka P 2001 Observation of the N_2 Herman infrared system in pulsed positive streamer induced emission at atmospheric pressure *J. Phys. D: Appl. Phys.* **34** 3185–90
[48] Lin X, Tyl C, Naudé N, Gherardi N, Popov N A and Dap S 2020 The role of associative ionization reactions in the memory effect of atmospheric pressure Townsend discharges in N_2 with a small O_2 addition *J. Phys. D: Appl. Phys.* **53** 205201
[49] Pipa A and Brandenburg R 2019 The equivalent circuit approach for the electrical diagnostics of dielectric barrier discharges: the classical theory and recent developments *Atoms* **7** 14
[50] Levasseur O, Stafford L, Gherardi N, Naudé N, Beche E, Esvan J, Blanchet P, Riedl B and Sarkissian A 2013 Role of substrate outgassing on the formation dynamics of either hydrophilic or hydrophobic wood surfaces in atmospheric-pressure, organosilicon plasmas *Surf. Coat. Technol.* **234** 42–47
[51] Pancheshnyi S V, Starikovskaia S M and Starikovskii A Y 2000 Collisional deactivation of $N_2(C\ ^3\Pi_u, v{=}0, 1, 2, 3)$ states by N_2, O_2, H_2 and H_2O molecules *Chem. Phys.* **262** 349–57
[52] Lafferty J M 1998 *Foundations of Vacuum Science and Technology* (New York: Wiley)
[53] Anon COMSOL Multiphysics®
[54] San O and Staples A E 2012 An improved model for reduced-order physiological fluid flows *J. Mech. Med. Biol.* **12** 1250052